Journal of Remote Sensing
A SCIENCE PARTNER JOURNAL

RESEARCH ARTICLE

Quantifying Cloud-Free Observations from Landsat Missions: Implications for Water Environment Analysis

Lian Feng* **and Xinchi Wang**

School of Environmental Science and Engineering, Southern University of Science and Technology, Shenzhen, China.

*Address correspondence to: fengl@sustech.edu.cn

Citation: Feng L, Wang X. Quantifying Cloud-Free Observations from Landsat Missions: Implications for Water Environment Analysis. *J. Remote Sens.* 2024;4:Article 0110. https://doi.org/10.34133/remotesensing.0110

Submitted 27 May 2023
Accepted 9 January 2024
Published 22 February 2024

Since the launch of the Landsat missions, they have been widely employed for monitoring water environments. However, the designed revisiting period of Landsat satellites is 16 days, leading to large uncertainties when tracking long-term changes in water environmental parameters characterized by high spatiotemporal dynamics. Given this challenge, comprehensive assessments of the global distribution of cloud-free observations (NCOs) obtained from Landsat missions and their applications in water environments and hydrology are currently unavailable. In this study, we utilized >4.8 million images acquired from Landsat-5, Landsat-7, and Landsat-8 to quantify and analyze the spatiotemporal variations of NCOs on a global scale. Our findings indicate that while NCOs demonstrate substantial spatial and temporal heterogeneities, Landsat-8 provides nearly twice as many mean annual NCOs (21.8 ± 14.7 year^{-1}) compared to Landsat-7 (10.8 ± 4.8 year^{-1}) and Landsat-5 (8.3 ± 5.6 year^{-1}). Moreover, we examined how the overlap area of adjacent orbits contributes to improving NCOs, noting that nearly all Landsat observation areas above 45°N are covered by overlapping paths in the east–west direction. Additionally, we conducted an analysis of the potential uncertainties arising from Landsat NCOs in obtaining long-term trends of various water parameters, including total suspended sediment (TSS) concentration, water level, water surface temperature (WST), and ice cover phenology. The results revealed that the uncertainty in water quality parameters (i.e., TSS) from Landsat is much higher than that in hydrological parameters (i.e., water level and WST). The quantification of NCOs and assessment of their impact on water parameter estimations contribute to enhancing our understanding of the limitations and opportunities associated with utilizing Landsat data in water environmental and hydrological studies.

Introduction

Satellite remote sensing plays a crucial role in monitoring the spatiotemporal dynamics of large-scale marine and freshwater ecosystems, primarily due to its advantage in data acquisition compared to traditional ship-based measurements. Coarse-resolution ocean color missions, such as sea-viewing wide-field sensor (SeaWiFS; 1997–2010), moderate-resolution imaging spectroradiometer (MODIS; 1999 to present), and medium-resolution imaging spectrometer (MERIS; 2002–2012) [1–4], as well as medium- to higher-resolution imagers like the Landsat and Sentinel series instruments, have been widely utilized to retrieve various water environmental parameters, including chlorophyll a, total suspended sediment (TSS), colored dissolved organic matter (CDOM), and water surface temperature (WST) [5–9].

However, unlike other land features, water bodies exhibit pronounced spatiotemporal dynamics, which pose higher temporal resolution requirements for monitoring water parameters. For instance, forest vegetation may not change substantially for weeks or even months [10,11], whereas water quality in inland or coastal areas can change dynamically within hours [12]. Therefore, insufficient observation frequency of remote sensing data may lead to substantial uncertainty in capturing short-term variations and long-term trends of water quality parameters. The magnitude of this uncertainty is determined by a variety of factors, including cloud coverage, the amplitude of changes in hydrodynamics, and biogeochemical processes within a short time period [13].

The effective oceanic observation by ocean color missions has been examined by several previous studies. For example, Feng and Hu [14] found that the global average daily percentages of valid observations (DPVOs) of the MODIS Level-3 chlorophyll a product were only about 5% (that is, only about 5 observations are valid out of 100 daily observations), mainly due to interference factors such as clouds, sunglint, and stray-light. In contrast, MODIS sea surface temperature retrievals are less affected by sunglint and other perturbations than chlorophyll a and normalized fluorescence line height (nFLH), resulting in much higher daily DPVOs [14]. Geostationary satellites have higher temporal resolutions, for instance, the first geostationary ocean color satellite mission [Geostationary Ocean Color Imager (GOCI)] can acquire eight satellite data per day, and its average DPVO in open ocean waters is 152.6%, which is 26 times that of MODIS [15].

Landsat satellites provide the longest record of earth observation data, and their higher spatial resolution compared to ocean color missions are better suited for inland and nearshore coastal water applications. However, the designed revisiting period of Landsat satellites is 16 days, which is much longer than the 1- or 2-day ocean color imagers, meaning that it introduces greater uncertainty in capturing the dynamics of aquatic ecosystems. For example, the mean number of cloud-free observations (NCO) for Landsat-5 TM observations is ~7.5 per year, and such observation frequency is impossible to accurately capture the interannual variability of lacustrine algal blooms [16]. Consequently, the global increasing trends of lake algal blooms detected by Ho et al. (2019) are subject to substantial uncertainty [17]. Additionally, the orbital characteristics of Landsat satellites also affect the revisiting period of observations. For example, the combination of Landsat-8 and Landsat-7 can reduce the revisiting period by half, and the overlap area of east–west neighboring orbits of one Landsat satellite has a revisiting period of 8 days [18,19]; these observation data can more effectively capture dynamic information on water environments.

Although Landsat has been widely applied in hydrological and environmental studies at spatial scales ranging from regional to global and temporal scales spanning half a century [20–22], the spatiotemporal distribution characteristics of Landsat's effective observation data currently lack a comprehensive evaluation, let alone the potential uncertainties caused by infrequent observation frequency. To fill such knowledge gaps, our studies aimed to (a) quantify the NCOs for three different Landsat missions, analyze the spatiotemporal variations of Landsat NCOs globally, and particularly investigate how the overlap area of east–west neighboring orbits can improve NCOs and (b) analyze the potential uncertainties introduced by cloud cover in obtaining long-term trends of various water parameters using Landsat, including TSS concentration, water level, WST, and ice cover phenology.

Materials and Methods

Satellite imagery

To evaluate the validity of observations, we utilized all Tier 1 TOA reflectance collections of Landsat-5, Landsat-7, and Landsat-8 that were archived in the Google Earth Engine platform. Data from Landsat-9 were not included due to its relatively short time period. We used all archived data of these missions between 1984 and 2020, with a total of 4,845,082 images globally; details regarding the number of images and dataset availability period for each Landsat mission are provided in Table1.

In situ measurements

To examine the capability of Landsat imagery in inland water studies, we examined four important parameters reflecting water environment and hydrological dynamics: TSS concentration,

Table 1. Total number of images used in this research summarized for Landsat-5, -7 and -8. All images are acquired from the Google Earth Engine platform.

	Number of images	Period
Landsat-5	1,661,079	03/19/1984-05/04/2012
Landsat-5	2,043,054	05/28/1999-12/31/2020
Landsat-5	1,140,949	03/18/2013-12/31/2020

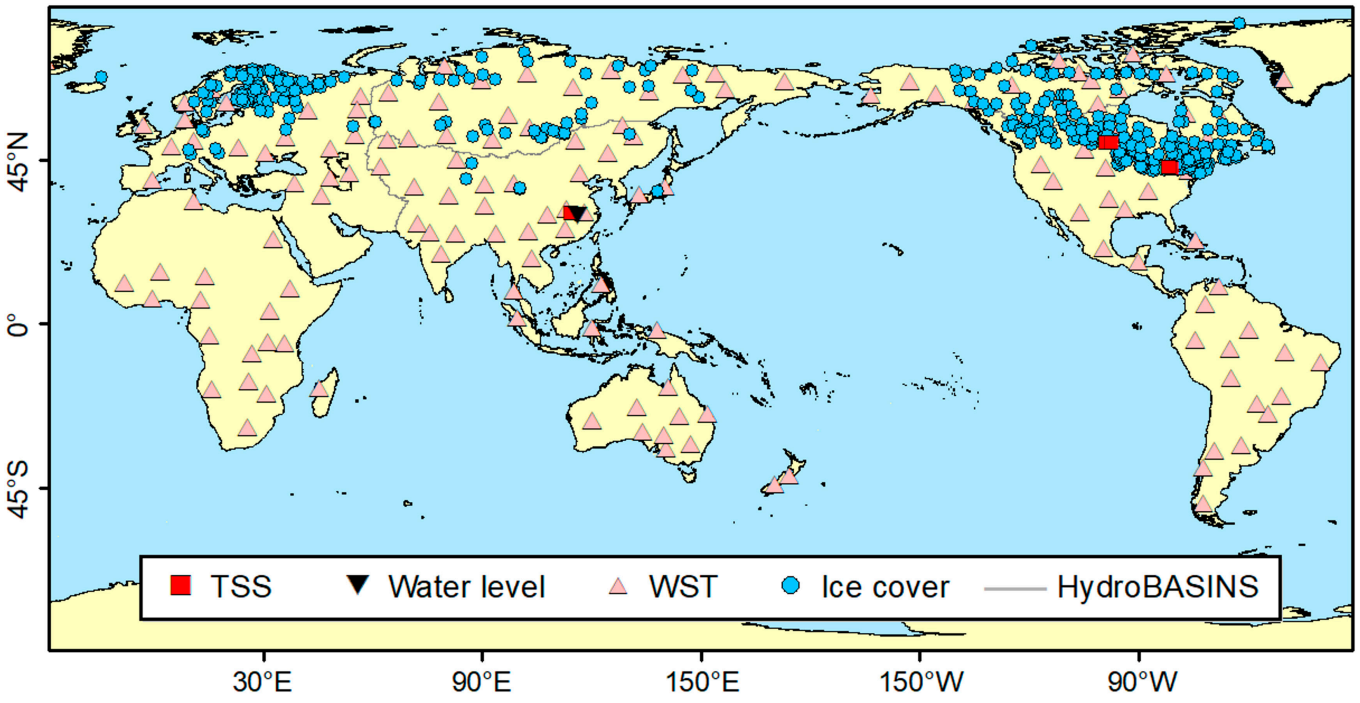

Fig. 1. Locations of in situ data for four water parameters examined in this study.

water level, WST , and ice cover phenology. All the in situ measurements were recorded on a daily basis, and the locations of the data are displayed in Fig. 1.

TSS is one of the three optically sensitive constituents that can be quantitatively retrieved using remote sensing observations and plays a crucial role in characterizing water quality [23–26]. In this study, in situ measurements from five hydrological stations were utilized due to their availability of complete multi-year data. One of the stations, located in the Yangtze River (Hankou station, 114.33°E, 30.63°N), was selected for its substantial short-term dynamics in sediment load. The data span from 1987 to 2001, except for 1989 and 1993, covering a total of 13 years. In addition, TSS measurements were also obtained from four hydrological stations in North America: Little Otter Creek (80.84°W, 42.71°N) from 1985 to 1996, Ausable River (81.66°W, 43.07°N) from 1985 to 1993, Assinibain River-1 (98.89°W, 49.70°N) from 1985 to 1996, and Assinibain River-2 (97.41°W, 49.87°N) from 1985 to 1991.

Water level is a key factor in reflecting the hydrodynamics of water bodies [23]. Although it is challenging for Landsat images to retrieve water level information, for water bodies with large dynamic changes, water level is highly correlated with their surface area and water storage [27,28]. Here, we assume that Landsat can extract water surface areas for highly dynamic water bodies, and this information can be characterized by water level. Our study only utilized one set of in situ measurements of water level; the data were obtained from a hydrological station located in Poyang Lake (116.03°E, 29.45°N), which is the largest freshwater lake in China [29]. The time period for the water level data was from 2002 to 2009, covering a total of 8 years. The inundation area of Poyang Lake shows dramatic seasonality, and the associated water level measurements exhibit an exceptionally wide water level range of up to 12 m [30], which indicates that satellite observations with infrequent temporal resolution may be subject to significant uncertainties when used to examine the lake's areal dynamics. Meanwhile, inland water bodies with relatively smaller water level fluctuations are expected to have less uncertainty when compared to this lake.

WST is a fundamental physical property of water bodies that is linked to their physical and chemical characteristics [31–34]. It affects the metabolism of aquatic organisms and is associated with various environmental problems [35–37]. In this study, WST data were obtained from the ERA5-Land Hourly reanalysis dataset on Google Earth Engine. The daily mean WST was computed by averaging the "lake mix layer temperature" band at four specific times (0:00, 6:00, 12:00, and 18:00). A total of 150 lakes were randomly selected from the GLAKES database [21], with 50 from each of the three groups categorized by lake area (less than 1 km^2, between 1 and 100 km^2, and larger than 100 km^2). For each lake, temperature obtained in the mixed layer was extracted from 1991 to 2020 (30 years) as the actual WST. Note that the spatial resolution of the ERA WST data is 11,132 m, which is larger than the spatial scale of most lakes [21]. However, in our analysis, the primary consideration is the consistency in the dynamic range and temporal trends between ERA WST and the actual lake temperatures, and the absolute differences between ERA WST and the observed lake temperatures do not affect the validity of our findings.

Ice cover on lakes or rivers is the fourth parameter studied in this research. The timing of lake ice events not only influences the annual life cycle of all organisms in these lacustrine ecosystems [38–40] but also affects recreational and economic opportunities for human society [41–43]. To investigate this parameter, we utilized in situ lake ice datasets provided by the Global Lake and River Ice Phenology Database (GLRIPD; version 1) [44]. Only data with complete glacial phenologies (ice-on and ice-off dates) within a year were retained, resulting in 480 in situ measurements. The locations of these measurements are mainly concentrated in the middle and high latitudes of the Northern Hemisphere, as shown in Fig. 1.

In this study, the HydroBASINS database [45] was employed for spatial zoning statistical analysis. This database provides global high-quality basin and sub-basin boundaries based on the Shuttle Radar Topography Mission (SRTM) digital elevation model [46]. Here, the level-1 product of HydroBASINS, which divides land into nine large watersheds (i.e., Africa, Arctic, Asia, Australia, Europe, Greenland, North America, South America, and Siberia), was utilized to explore the differences in observation quantities across different watersheds.

Calculation of the number of valid observations

The first step in our analysis was to calculate the global annual average number of total observations (NTOs) for Landsat-5, Landsat-7, and Landsat-8 at the pixel level (Table 1). We then computed the NCOs for the three Landsat missions utilizing NTOs, whereby pixels impacted by cloud cover, cloud shadows, and other factors were designated as invalid. We used the Fmask algorithm to identify invalid pixels. The Fmask algorithm categorizes each Landsat pixel into distinct classes, including cloud-free, cloud, and cloud shadow [47]. The classification results have been incorporated into the quality band of Landsat image, which is the Quality Assessment 16-bit band associated with each image (https://www.usgs.gov/landsat-missions/landsat-collection-1-level-1-quality-assessment-band). We used the Quality Assessment band from Tier 1 TOA reflectance collections to determine whether pixels are valid or not. Specifically, we considered radiometric saturation bits 2 to 3, cloud confidence bits 5 to 6, and cloud shadow confidence bits 7 to 8 for Landsat-5 and Landsat-7. If any one of the above double bits is "11," indicating a high confidence (67% to 100% confidence) that the condition (cloud or cloud shadow) exists, or five or more bands contain saturation, the pixel is deemed "invalid." For Landsat-8, the criteria for determining cloud, cloud shadow, and radiometric saturation are similar to Landsat-5 and Landsat-7, but additional double bits 11 to 12 are used to consider cirrus confidence. If the cirrus confidence double bits are "11," the pixel is also considered "invalid." It is important to note that in addition to cloud coverage, other factors such as sunglint and straylight, among others, could also impact the reliability of satellite observations for water applications [14]. However, the definitions of these factors may differ across different instruments or water constituents. For the purpose of our study, we focused on evaluating the effects of cloud contamination on the observations.

Overlaps of adjacent Landsat paths can significantly affect both NCOs and NTOs. Notably, overlaps occur in both north–south and east–west directions. In the case of east–west overlaps, the temporal interval between multiple observations of the same pixel is generally 8 days. This phenomenon leads to an increase in NCOs and a decrease in the revisiting period to approximately 8 days, deviating from the nominal value of 16 days. To investigate the distribution of overlaps at different latitudes and their impact on NCOs and NTOs in various regions, we calculated the ratio of overlapping pixels to the

total number of pixels. The ratio of overlapped regions is primarily related to latitude, with high-latitude regions experiencing a shorter earth circumference and larger overlap coverage. It is worth noting that the time interval for north–south overlaps is typically very short, lasting only a few minutes. Therefore, duplicate observations of the same pixel during this time interval should be considered a single observation. In this regard, unless otherwise specified, the term "overlap" mentioned later in this paper refers to the overlap in the east–west direction.

Assessment of the impact of NCOs on inland water applications

Within the periods when continuous in situ data are available, we identified the days when "cloud-free observations" from Landsat were obtainable. Subsequently, we calculated the mean value of the parameters during these time periods using the in situ measurements. Additionally, we calculated a separate annual mean value for the same parameters using only the in situ data corresponding to the dates of Landsat cloud-free observations, and these annual mean values were assumed to represent the data that can be accurately acquired by Landsat. In light of our assumption that parameters observed or retrieved from Landsat images were entirely accurate, any differences between the two annual mean calculations were attributed to the limitation of infrequent satellite observations. We utilized two indicators to quantify the differences: (a) the mean annual absolute percentage error (MAPE), calculated as the mean of the absolute differences between satellite and in situ estimated annual values, and (b) the differences in their associated trends, where the trends were represented by the linear slopes across the examined period.

We further calculated the relationships between the uncertainties of satellite retrievals and NCOs for different parameters by the following processes: First, we obtained NCOs and the in situ mean value of the water environmental parameters for each year. Second, we calculated the annual mean value of the examined parameters that can be obtained by the satellite (i.e., annual mean values estimated using in situ measurements taken at the time when cloud-free Landsat images were available). Finally, we computed the difference (in absolute or relative) between satellite observation and the in situ observation for all examined years, both inside and outside the overlaps. Given the substantial variability in the NCOs observed in different years, our analysis of long-term annual data enabled us to evaluate the potential influence of NCOs on the annual-scale uncertainty of satellite data, represented as the disparity between in situ measurements and satellite retrievals.

The impact of east–west overlaps on NCOs can lead to large differences even between observation locations that are in close proximity to each other. This is particularly true when one location is situated inside the overlap region while the other is outside of it. To provide a more comprehensive evaluation of the impact of NCOs, we selected five additional observation locations for TSS-measured stations and one additional observation location for water level-measured stations (Fig. 2). Each of these locations was chosen in close proximity to the original station (within 100 km), but was situated either inside or outside the overlap region, depending on the opposite condition of the original station. This allowed us to compare the differences in the impact of NCOs between inside and outside the overlap region.

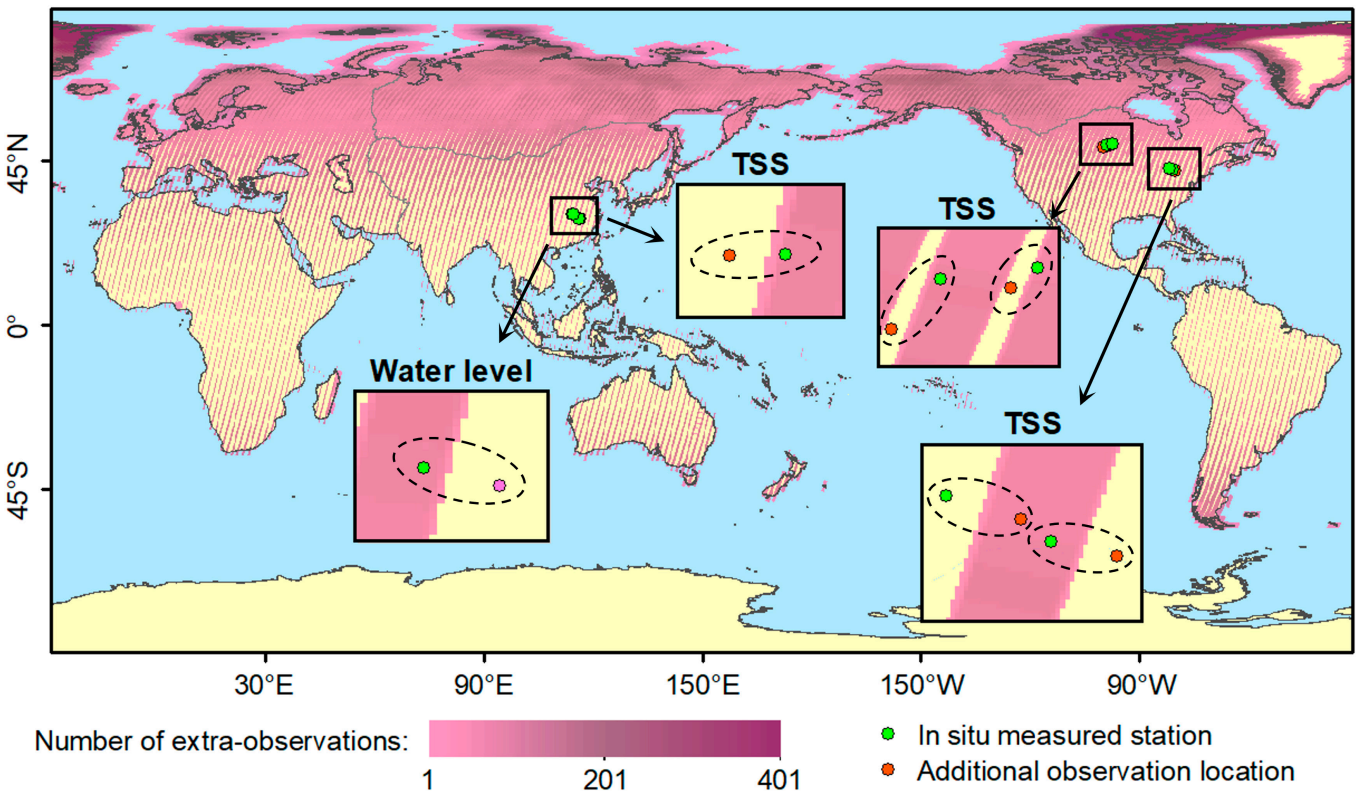

Fig. 2. Locations for hydrological measured stations and additional observed locations inside or outside the overlap region. The background represents the number of extra-observations provided by the overlaps of adjacent Landsat paths in the east–west direction.

In order to investigate the impact of NCOs on Landsat-derived water parameters, it is imperative to consider the availability of Landsat archives over different time periods. However, we faced the challenge of limited in situ measurements at a daily scale for certain time periods, particularly for TSS and water levels. To address this challenge, we shifted the in situ measurements of TSS and water level a few years earlier or later. For instance, the in situ water level measurements at Xingzi station were only recorded between 2002 and 2009, but we shifted these measurements to the periods of 1987–1994 and 2013–2020. In other words, the water levels for these shifted periods (1987–1994 and 2013–2020) are assumed to be identical to the measurements obtained during the actual recorded years (2002–2009). When analyzing Landsat-5, we obtained the trend from satellite observations between 1987 and 1994 and compared it with corresponding trend from shifted in situ data. This allowed us to assess whether the NCOs of Landsat-5 during 1987–1994 could effectively capture water level trends. Similarly, we employed shifted data from the period of 2013–2020 to evaluate the ability of Landsat-7 and Landsat-8 to capture water level trend. This approach allows us to analyze the ability of three Landsat missions to retrieve water level information during these shifted periods, even in the absence of actual measured data during those time periods. Certainly, the feasibility of this approach is contingent upon a crucial assumption: we assume that Landsat's quantitative inversion algorithms for water parameters are error-free. Hence, the specific period of the in situ measurements is not of paramount importance. Our analysis primarily focuses on examining the disparity between the effective data sampling frequency in Landsat and the trends obtained from daily in situ measurements.

A commonly used approach for water parameters is to combine multiple years of observations to obtain the average condition of the parameter during the period, which is generally represented by the percentage of occurrence [22,35,48]. The calculation of occurrence is the number of times a phenomenon (i.e., water inundation, algal bloom, and ice coverage) occurs during the period divided by the number of valid observations. The effectiveness of this approach and the uncertainties caused by combining varied numbers of years are also discussed in this study using the GLRIPD dataset.

Results

Annual mean NTOs, NCOs, and their ratio for different Landsat missions

The global mean annual NTOs for Landsat-5, Landsat-7, and Landsat-8 are displayed in Fig. 3. Landsat-8 shows the highest frequency of observations with a mean value of 34.5 ± 17.3 times per year (year^{-1}). Landsat-7 follows with a mean value of 16.1 ± 5.9 year^{-1}. Meanwhile, Landsat-5 has the lowest frequency of observations with a mean value of 12.0 ± 7.5 year^{-1}. The observations from Landsat-5 are mainly concentrated in several areas, such as central North America, central South America, Europe, southwest Asia, eastern Asia, and Australia, while they are unavailable in some regions, such as Alaska, Central Africa, and northeast Russia. In contrast, observations from

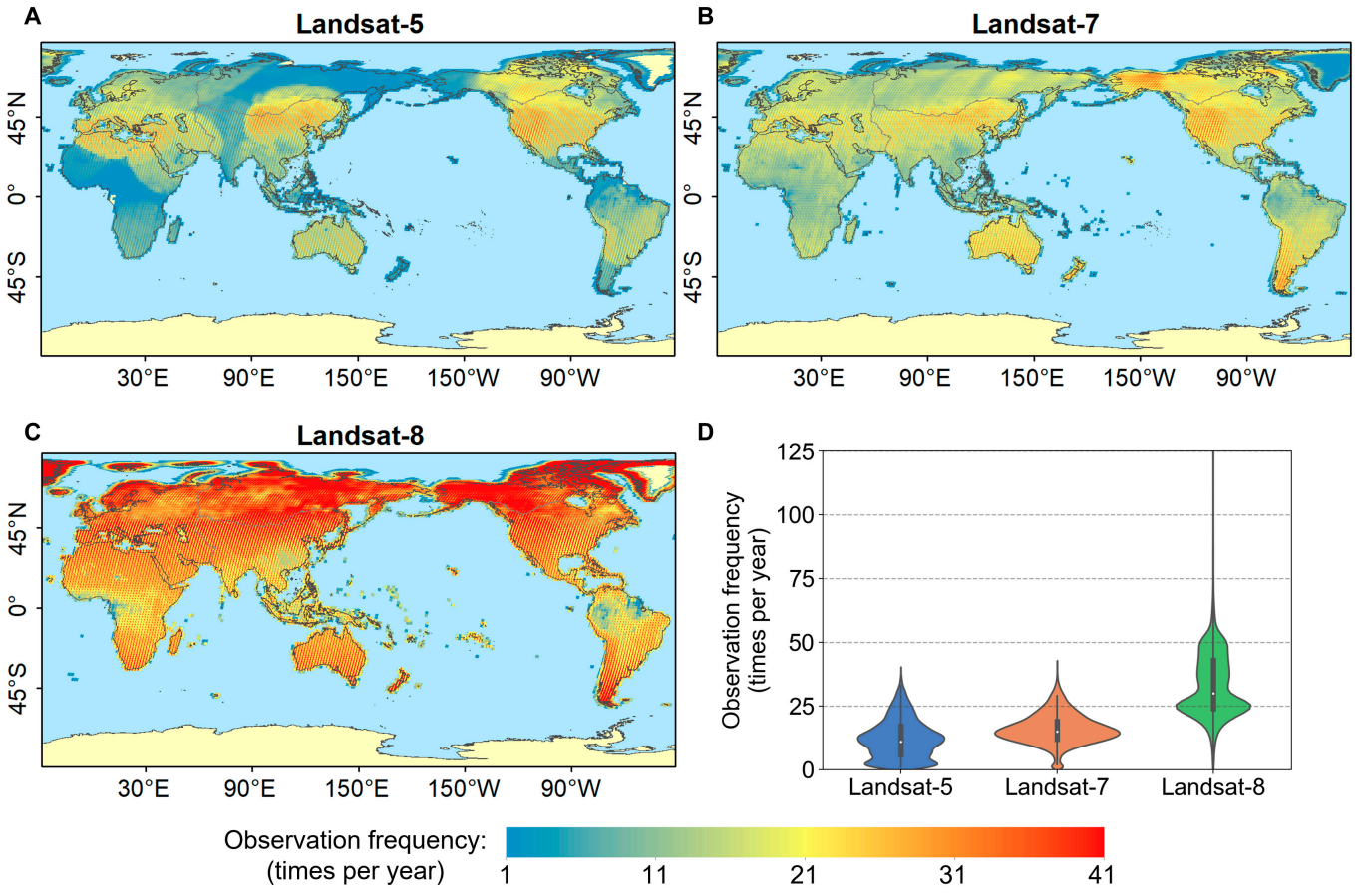

Fig. 3. Global annual mean NTOs for (A) Landsat-5, (B) Landsat-7, and (C) Landsat-8. (D) Violin plot of the distributions of NTOs in times per year (year^{-1}).

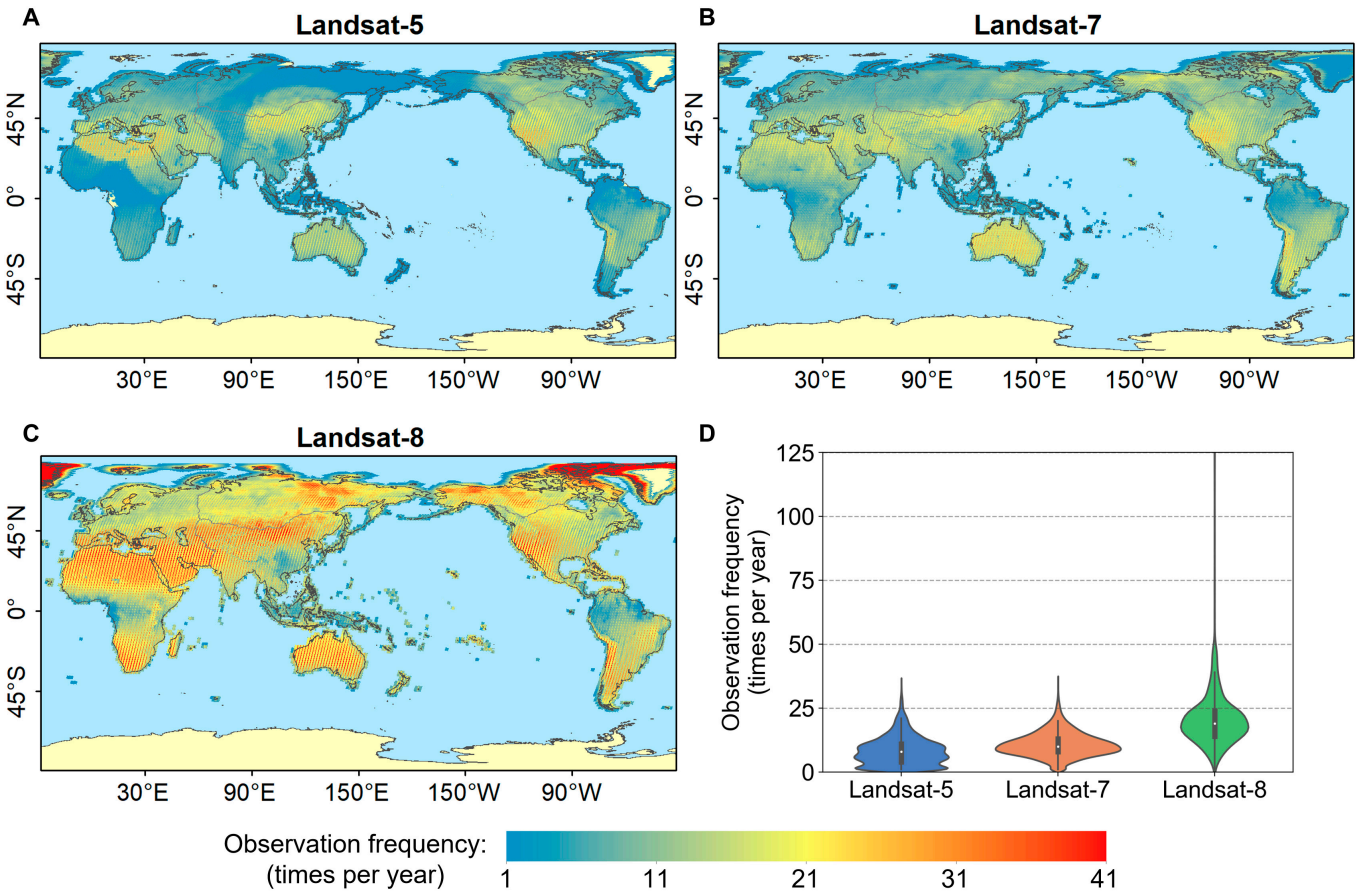

Fig. 4. Global annual mean NCOs for (A) Landsat-5, (B) Landsat-7, and (C) Landsat-8. (D) Violin plot of the distributions of observation frequency in times per year.

Landsat-7 and Landsat-8 are more uniform and cover almost all land areas except for Antarctica.

The global mean annual NCOs for different Landsat missions are illustrated in Fig. 4. The global spatial patterns of NCOs aligned well with that of NTOs. Numerically, Landsat-8 has nearly twice as many mean annual NCOs (21.8 ± 14.7 year^{-1}) compared to Landsat-7 (10.8 ± 4.8 year^{-1}) and Landsat-5 (8.3 ± 5.6 year^{-1}).

The ratio of NCOs to NTOs from different Landsat missions is presented in Fig. 5. The global spatial distribution of the NCO/NTO ratio is consistent for all three missions, as it is mainly influenced by the local climate's cloud probability. Regions with dry climates, such as southern Africa, northern Africa, southern Europe, and central Australia, tend to have relatively high valid ratios (Fig. 5A to C). The global mean valid ratio for Landsat-8 is 61.7% (median = 60%, Fig. 5D), which is consistent with the global average cloud-free frequency [49].

To investigate the valid observations of Landsat missions on various watersheds worldwide, we utilized HydroBASINS level-1 polygon data, which divide the global land into nine large watersheds (Fig. 6A). These watersheds include Africa, Arctic, Asia, Australia, Europe, Greenland, North America, South America, and Siberia. Besides NTOs and cloud coverage, the percentage of overlapped regions is another crucial factor affecting NCOs. Figure 6A to C shows the spatial pattern of overlapped regions for the entire globe and two regions (regions 1 and 2). Region 1 is a typical low-latitude area located at the northern end of South America with a latitude range of −2°N to 13°N (Fig. 6B). The longitude span of overlap in region 1 is approximately 0.2° to 0.3°. Region 2 is located in the center of Eurasia, with a relatively high latitude ranging from 43°N to 58°N (Fig. 6C). The longitudinal span of overlap in region 2 is approximately 0.7° to 0.9°, and the areas above 54°N are fully covered by overlap from adjacent Landsat paths. Figure 6D illustrates the latitudinal distribution of the ratio of overlap area to observational area from three Landsat missions. On the equator, the overlap ratios of Landsat-5, Landsat-7, and Landsat-8 are 16.5%, 20.3%, and 14.7%, respectively. The area of overlap increases significantly from the equator to the pole. The latitudinal profiles of the percentage of overlap regions of the three Landsat missions are almost identical, with slight deviations caused by the Landsat sensor orbits' drift primarily due to Earth's gravitational effects [50]. Above 51°N, almost all (>99%) Landsat observational areas are covered by overlapped paths in the east–west direction.

The NCOs within and outside the overlapped regions for three Landsat missions in nine large watersheds are compared in Fig. 7. For regions situated at middle and low latitudes, such as Africa, Asia, Australia, South America, and North America, NCOs inside the overlap areas are considerably higher than those outside the overlap. Conversely, for regions located at high latitudes, such as Arctic, Greenland, and Siberia, nearly all observations for the three Landsat missions are derived from overlap regions and remain at relatively high frequency. In Europe, the frequency of observations within the overlapping regions is lower compared to those outside. This is due to the lower NCOs of

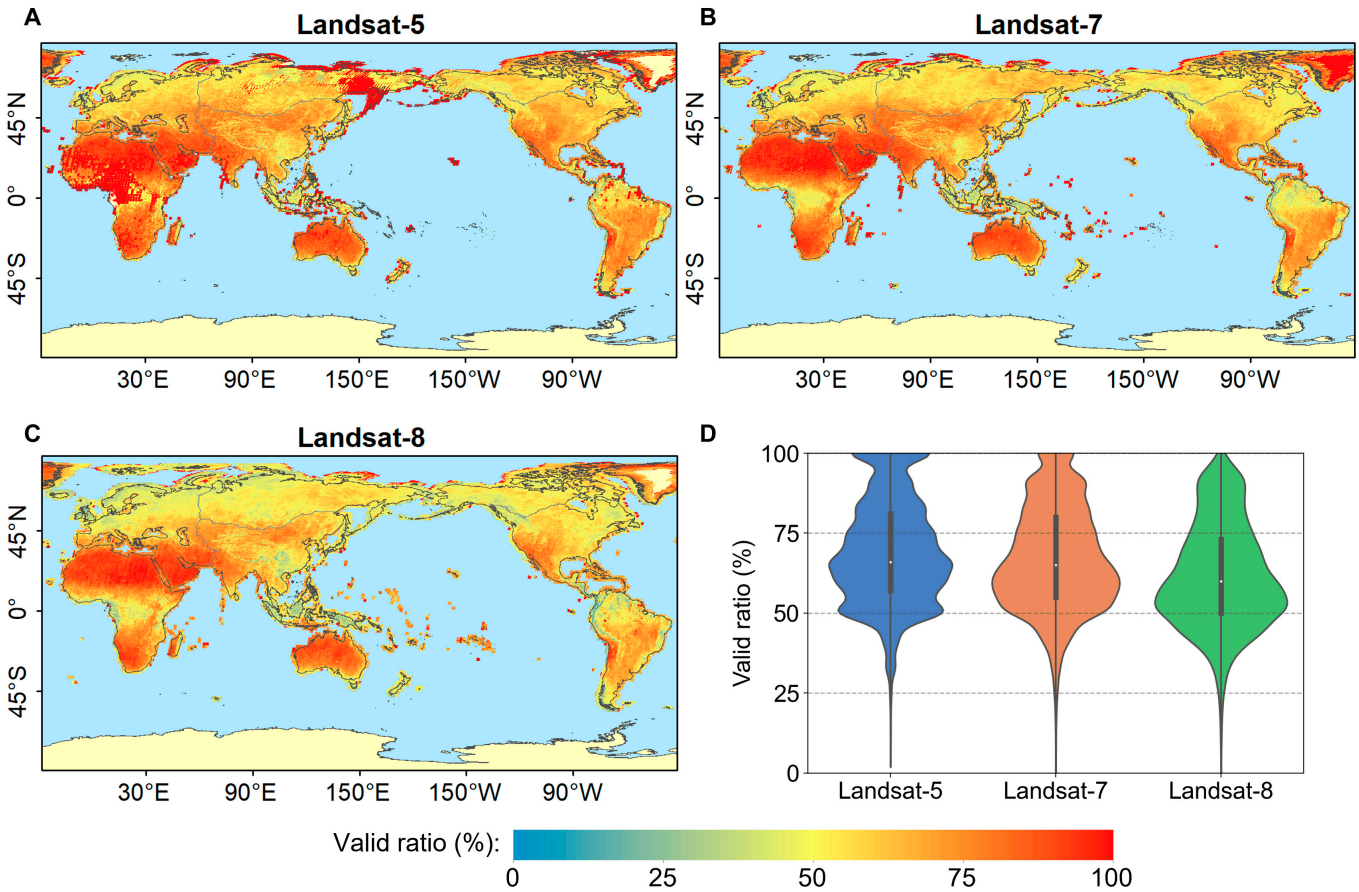

Fig. 5. Ratio of NCOs to NTOs for (A) Landsat-5, (B) Landsat-7, and (C) Landsat-8. (D) Violin plot of the distributions of ratio values in percentage.

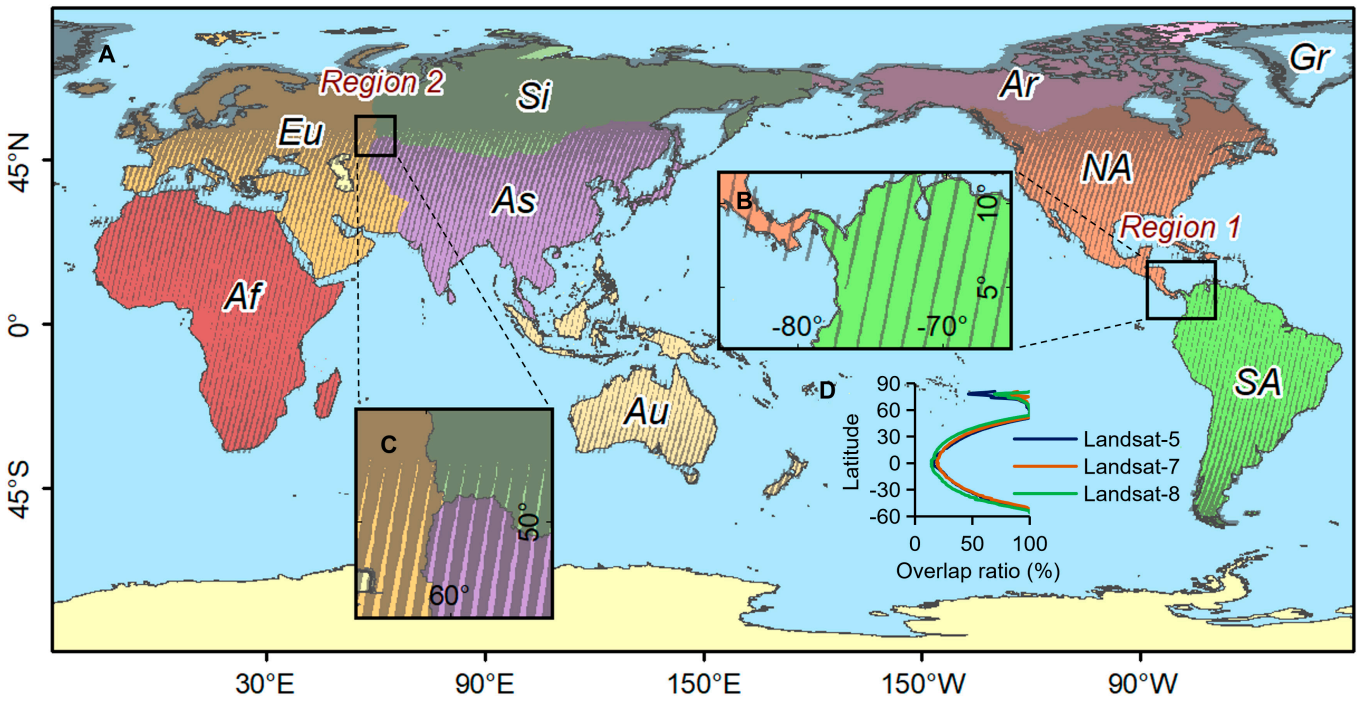

Fig. 6. (A) Nine global water basins from HydroBASINS level-1 polygon data and global spatial pattern of overlapped regions. (B) Local pattern of overlap in region 1. (C) Local pattern of overlap in region 2. (D) Latitudinal distribution of the ratio of overlap area to observational area from three Landsat missions. Af, Africa; Ar, Arctic; As, Asia; Au, Australia; Eu, Europe; Gr, Greenland; NA, North America; SA, South America; and Si, Siberia.

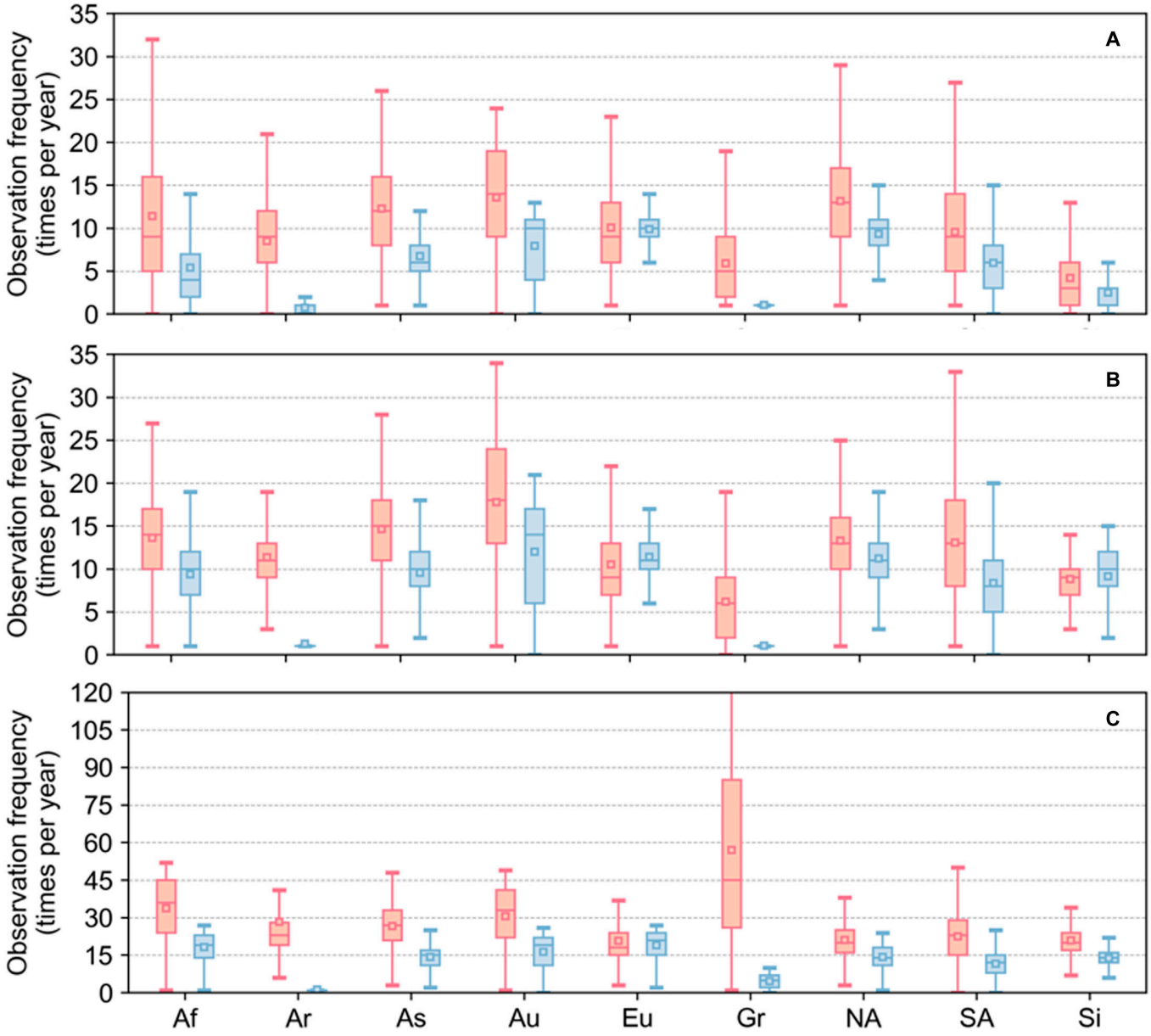

Fig. 7. Impact of overlaps on NCOs for (A) Landsat-5, (B) Landsat-7, and (C) Landsat-8 in nine regions. The box in pink/blue color represents the statistics inside/outside the overlaps of the adjacent Landsat paths.

Landsat missions in northern Europe (as shown in Fig. 4) and the fact that this region is entirely inside the overlap.

Intra- and interannual changes of the NCOs

Using Landsat-8 as an example, Fig. 8 and Table 2 illustrate the intra-annual or monthly variation in NCOs. The global NCOs display substantial seasonality and strong spatial heterogeneity. Regions exhibiting high values (>0.5) of the coefficient of variation (CV), calculated by dividing the standard deviation of 12 monthly climatologies by their mean, are predominantly located in northern South America, Central Africa, and southwest Asia, aligning with global precipitation patterns. Furthermore, the high latitudes of the Arctic exhibit elevated CV values due to the presence of polar darkness during winter months. These findings underscore the importance of considering substantial seasonality when calculating the annual average mean value of water environmental parameters, particularly in regions characterized by high CV.

The interannual changes in NTOs and NCOs for three Landsat missions from 1984 to 2020 are shown in Fig. 9. The NTOs and NCOs are primarily influenced by the number of satellites in orbit, the operational status of instruments, and the number of ground base stations [51,52]. Landsat-5 started acquiring images in 1984 [52]. With the use of more ground base stations, the acquisition volume increased annually, from 4.4 $year^{-1}$ in 1984 to 14.2 $year^{-1}$ in 1998 for Landsat-5. The global average NTOs increased sharply in 1999 and 2013, with Landsat-7 and Landsat-8 respectively obtaining data reaching 20.2 $year^{-1}$ and 35.4 $year^{-1}$. Landsat-5's decommissioning on 2013 June 19 resulted in small values in NTO and NCO in 2012 [53]. On 2003 May 31, the Scan Line Corrector (SLC) of Landsat-7 failed, causing about 22% of missing data [51,54,55]. However, in the same year, many regions had re-enabled the reception of Landsat-5 data, increasing the valid observations of Landsat-5 data since then. For Landsat-5, Landsat-7, and Landsat-8, the global average NTOs (NCOs)

Table 2. NCOs in nine global major watershed boundaries for 12 climatological months (i.e., long-term monthly mean, in times/month). Also listed are their mean (Avg.), standard deviation (Std.) and coefficient of variation (CV). Af: Africa, Ar: Arctic, As: Asia, Au: Australia, Eu: Europe, Gr: Greenland, NA: North America, SA: South America, and Si: Siberia.

	Af	Ar	As	Au	Eu	Gr	NA	SA	Si
Jan.	1.5	0.5	1.4	1.3	0.9	0.0	1.1	0.9	0.7
Feb.	1.4	1.2	1.3	1.2	1.0	0.2	1.0	0.8	1.2
Mar.	1.5	2.2	1.5	1.4	1.3	1.7	1.2	0.9	1.5
Apr.	1.5	3.1	1.4	1.4	1.5	3.9	1.3	0.8	1.6
May.	1.6	3.2	1.4	1.5	1.7	5.3	1.4	0.9	1.6
Jun.	1.6	2.9	1.2	1.4	1.8	5.5	1.4	1.0	2.2
Jul.	1.6	2.9	1.2	1.5	2.0	6.0	1.6	1.2	2.1
Aug.	1.5	2.2	1.2	1.6	1.9	4.9	1.5	1.3	1.8
Sep.	1.5	2.0	1.4	1.6	1.7	3.5	1.3	1.2	1.4
Oct.	1.5	1.2	1.6	1.5	1.3	0.7	1.2	1.1	1.1
Nov.	1.4	0.7	1.4	1.4	0.9	0.1	1.0	0.8	0.8
Dec.	1.5	0.3	1.5	1.3	0.8	0.0	1.0	0.9	0.4
Avg.	1.5	1.9	1.4	1.4	1.4	2.7	1.3	1.0	1.4
Std.	0.07	1.01	0.12	0.11	0.41	2.33	0.18	0.17	0.53
CV	0.04	0.54	0.08	0.08	0.29	0.88	0.15	0.17	0.39

during service are 11.5 (7.7) year^{-1}, 14.9 (9.8) year^{-1}, and 28.1 (17.5) year^{-1}, respectively. Nonetheless, for some areas and periods, observations may be less or missing, such as Arctic, Australia, and Greenland. For instance, the average NCOs of Landsat-5 in Australia are 9.5 year^{-1}, but only 0.5 year^{-1} from 2001 to 2003.

Capability in tracking long-term changes for different parameters of inland waters

The capability of Landsat in tracking TSS concentration inside and outside the observation overlapped region for five data series from four rivers is displayed in Fig. 10. The measured data are on a daily scale between 1985 and 2002. To further investigate whether adding Landsat-8 observation has improved the accuracy of tracking TSS, five additional series of data were obtained by shifting the year. Our results confirmed that the increased data volume from Landsat-8 reduces the discrepancies between satellite and in situ derived trends for all five series of data.

TSS may exhibit rapid short-term dynamics, increasing by orders of magnitude within a few days before decreasing rapidly. This poses a challenge for Landsat to accurately capture TSS concentrations, resulting in errors between the estimated interannual trends and actual conditions. The mean value of observed MAPE inside and outside the observation overlap is 14.6% and 21.1%, respectively. However, more NCOs do not always result in more accurate results. For instance, in the second observation station on Assinibain River (Fig. 10J), the slope calculated from the observation outside the overlap is closer to the real situation, with a lower MAPE of 6.9% compared to 12.9% from that inside the overlap. This is because, in some

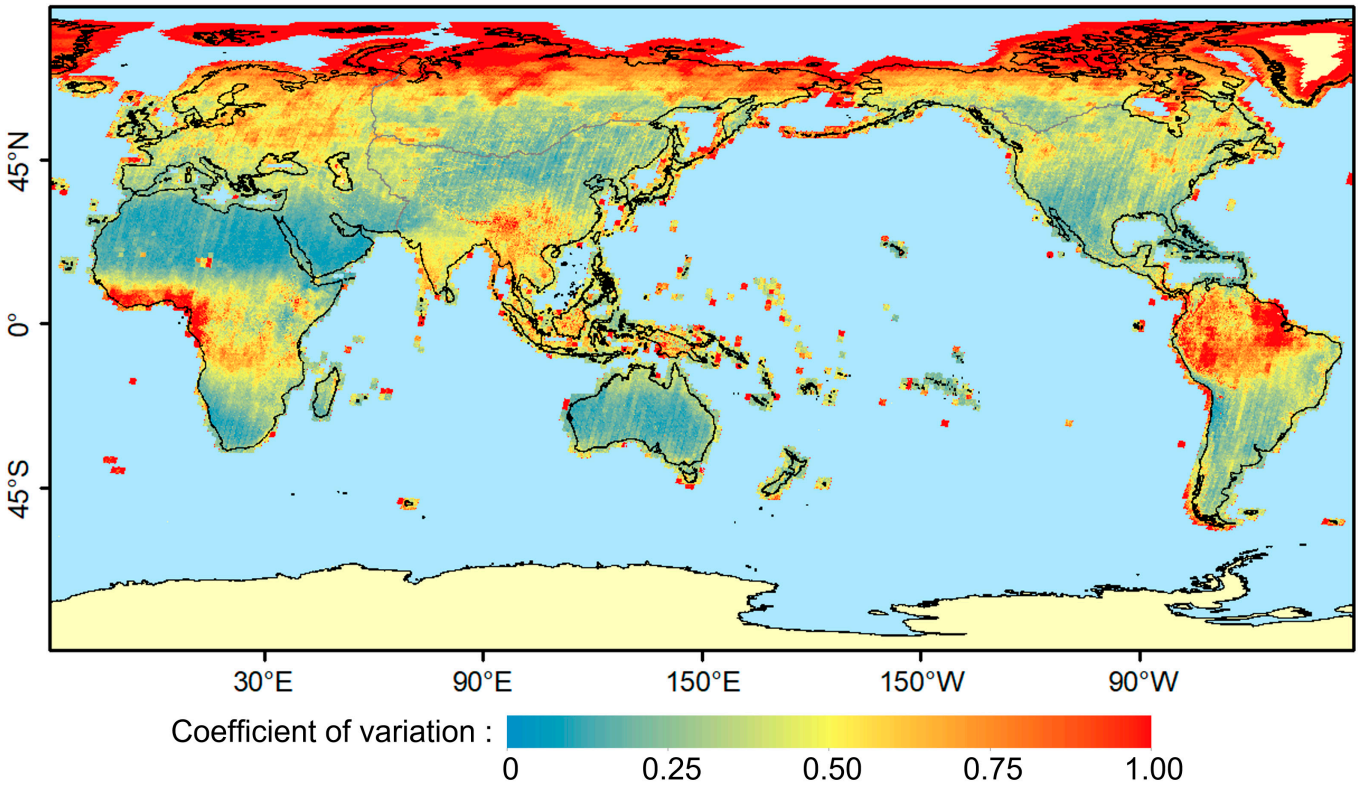

Fig. 8. Global pattern of monthly variation in NCOs for Landsat-8, represented as the coefficient of variation of 12 monthly climatologies.

years, more valid observations are concentrated in the high values (i.e., data distribution is not even), leading to the deviation of long-term trends. Figure 10K also shows how NCOs could impact the uncertainty of annual mean TSS values. When NCOs are less than 10 year^{-1}, the mean difference of annual mean TSS between satellite and in situ data is 23.6%. When NCOs exceed 10, 20, and 30 year^{-1}, the mean difference is reduced to 17.3%, 12.3%, and 10.4%, respectively.

We investigate the dynamics of water level, a key indicator for surface area of Poyang Lake. The annual values between satellite and in situ water levels show small differences (MAPE < 6%) (Fig. 11A to C). The box plot in Fig. 11D displays the uncertainty of water level as a function of NCOs, which reveals a significant decrease in mean difference between in situ and satellite retrievals as NCOs increase. To calculate the accurate annual mean change trend of water level over 8 years (−0.28 m year^{-1}), we

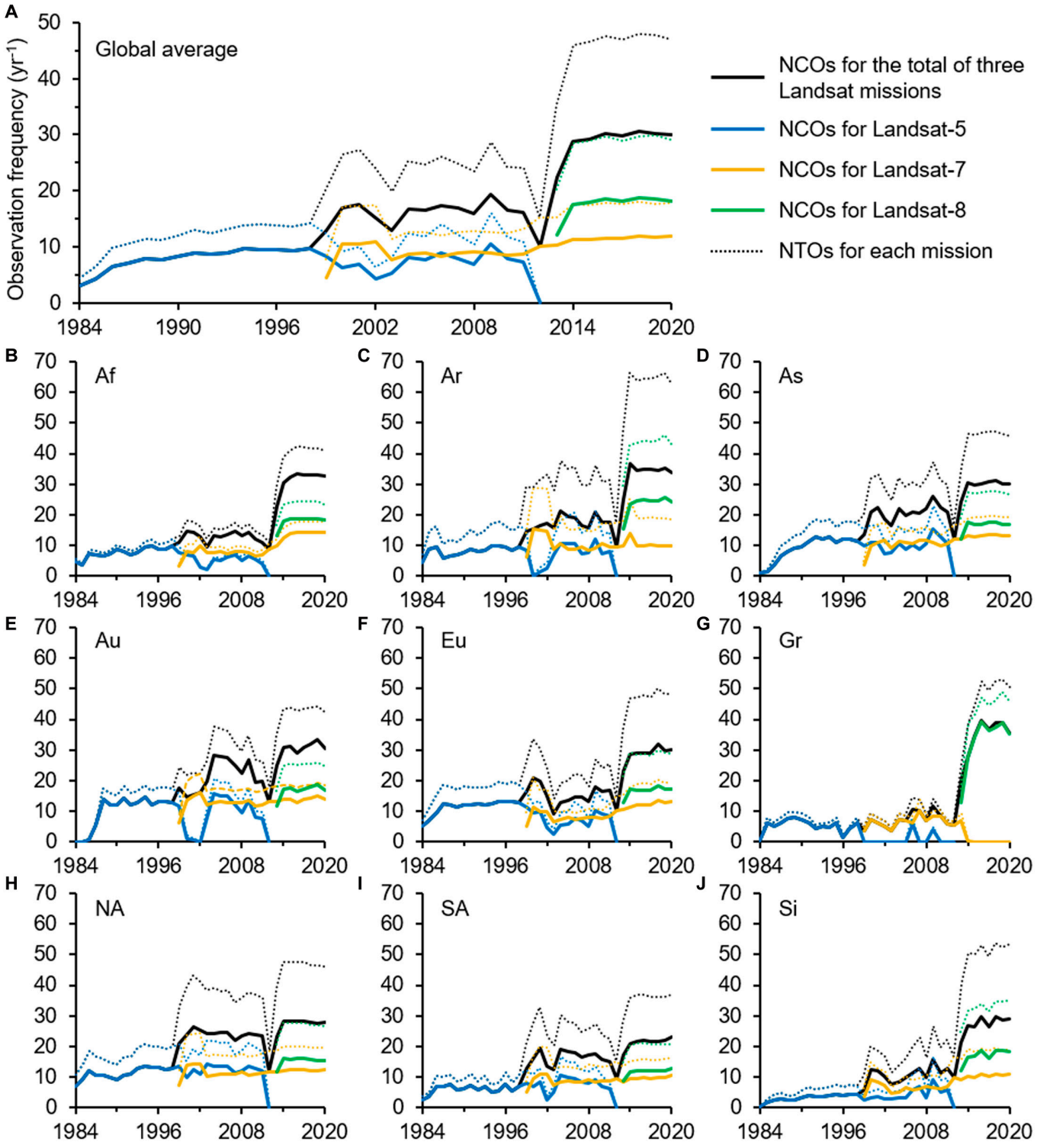

Fig. 9. (A) Global and (B to J) regional average NTOs and NCOs for three Landsat missions.

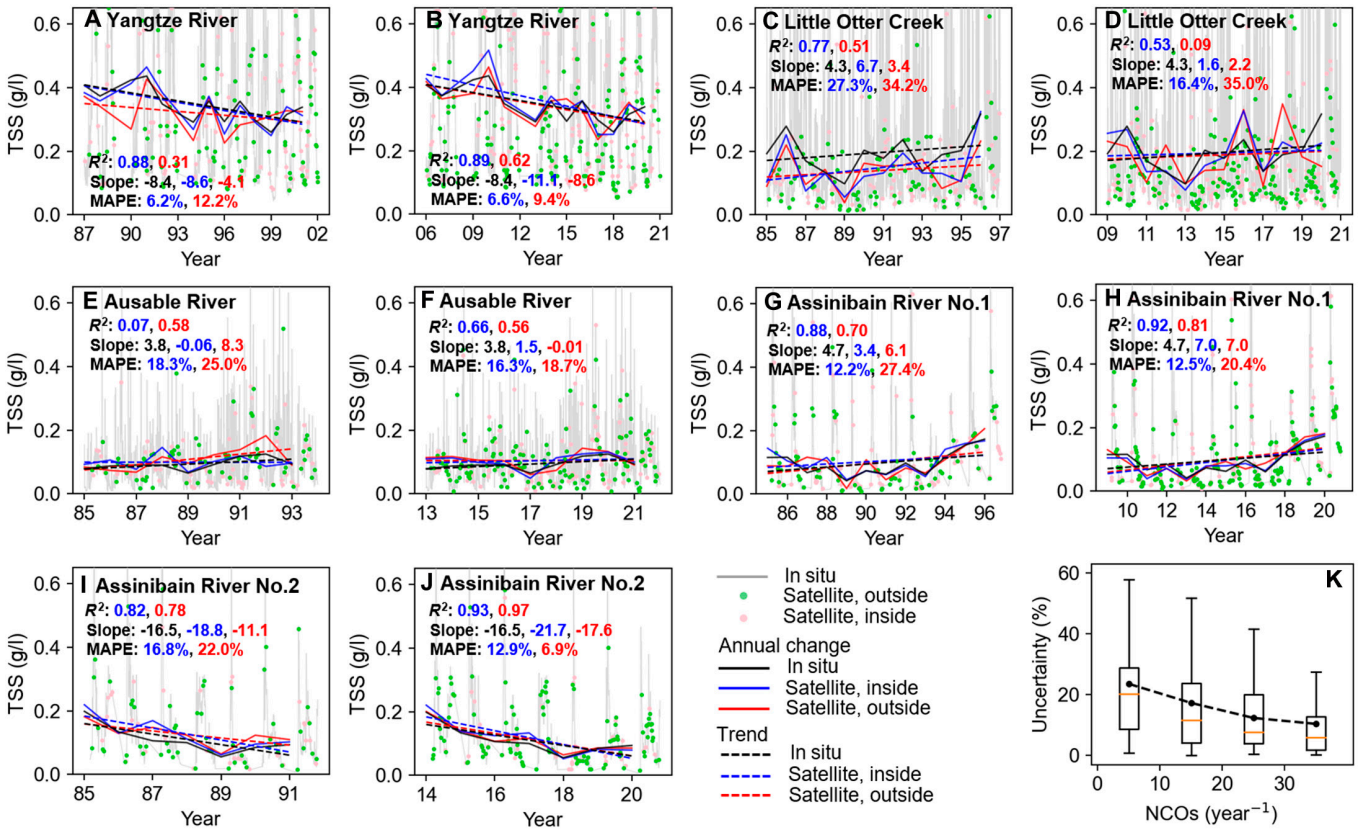

Fig. 10. Long-term TSS concentration measurements and valid observations using the combination of Landsat-5, Landsat-7, and Landsat-8 on (A and B) Yangtze River, (C and D) Little Otter Creek, (E and F) Ausable River, and (G and H) Assinibain River. (I and J). Left and right panels for each pair are original and shifted series. In each panel, the light gray line represents the in situ measured daily TSS concentration data. Dots represent valid observations from Landsat on that day (green for observations outside the overlap and pink for extra-observations inside the overlap). Annual changes (solid line) and their trends (dashed line) of in situ measured data (black color); observations inside the overlap (blue color) and outside the overlap (red color) are also shown, along with the corresponding statistical metrics (R^2, slope of trend, and MAPE). (K) Box plot chart for the relationship between NCOs and the uncertainty of annual mean TSS concentration.

use in situ measured daily water level data in Fig. 11A to C. We also estimate the trend inside/outside the observation overlap (in blue/red) in different periods. Inaccurate mean water level values for each year can eventually lead to errors in multi-year trends. The results show that during the period of 2013–2020, which had the highest average NCOs, the trend error was only 0.01 m year^{-1}. Conversely, using the same measured data, observations outside of the overlap during the 1987–1994 period, which had the least average NCOs, will result in a slope error of 0.19 m year^{-1}, which is 19 times larger.

WST is a fundamental physical parameter of inland waters and is commonly used to measure the impact of climate change on water environments. To explore the impacts of Landsat NCOs on the accuracy of WST monitoring, we utilized WST data from the ERA5-Land Hourly reanalysis dataset from 150 lakes between 1991 and 2020 (see Materials and Methods, Fig. 1). We plotted the differences between in situ and satellite WST, in terms of both relative and absolute values, as a function of NCOs (Fig. 12). The relative difference of WST can reach 2.5 °C when NCOs are <5 year^{-1}, but can be as high as 12.9 °C for some lakes. As NCOs increase, the differences decrease rapidly. For NCOs exceeding 5, 10, 15, and 20 year^{-1}, the annual mean difference of WST decreases by 41.0%, 57.8%, 66.6%, and 79.2%, respectively (Fig. 12A). The global average NCO from 1984 to 2020 is 15.5 year^{-1}, which suggests that the uncertainty associated NCOs for annual mean Landsat WST is around 0.9 °C. Moreover, we also used WST data to estimate the trend differences caused by Landsat NCOs in three 10-year periods of 1991–2000, 2001–2010, and 2011–2020 (Fig. 12B). Within a 10-year period, when the average NCO is less than 5 year^{-1} and between 5 and 10 year^{-1}, the average trend differences caused by NCOs are 0.19 and 0.17 °C year^{-1}, respectively. When NCOs exceed 10 year^{-1}, the mean trend difference is stable at 0.1 °C year^{-1}, and there is almost no further decrease with an increase in NCOs ($\Delta < 0.01$ °C year^{-1}).

Ice cover, an indicator of climate change in water environments, is highly sensitive to variations in climate [22,56]. We observed that when the NCO is less than 5 year^{-1}, the annual mean difference between satellite and in situ ice cover occurrence (ICO) is as high as 29.0% (Fig. 13). When NCOs exceed 20 year^{-1}, the difference decreases to 7.5%, but still has a substantial impact on the accuracy of ICO estimates. The mean NCO of combined Landsat data for all in situ measured inland water bodies is 5.1 year^{-1}, resulting in a high difference of 13 to 29%. Furthermore, we found a linear relationship ($R^2 = 0.99$) between the number of combined years in a period and the corresponding NCOs (blue dotted line), with NCOs increasing by about 7.4 for each additional year of Landsat data. The ICO difference decreases by 7.4%, 10.4%, 12.2%, and 13.4% when combining data for 2, 3, 4, and 5 years, respectively. However,

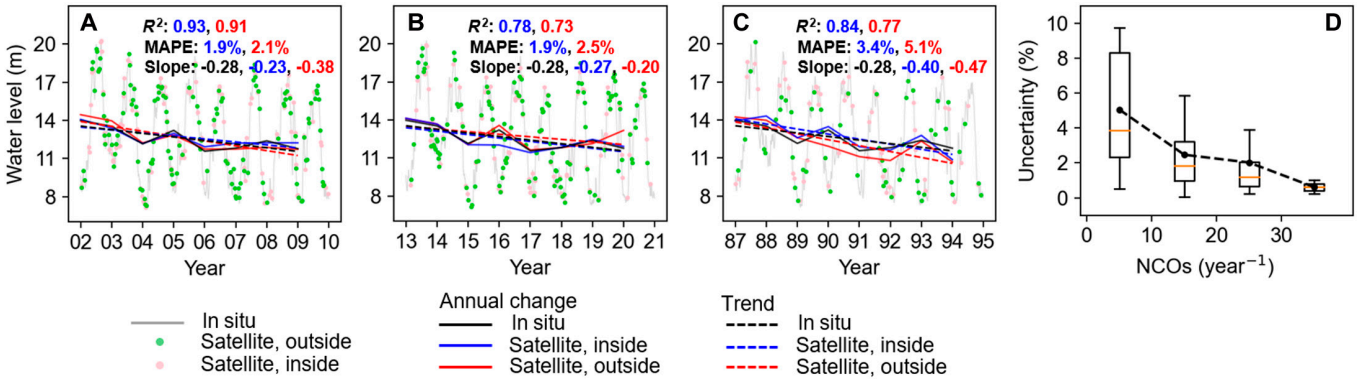

Fig. 11. (A) Long-term water level measurements and valid observations using the combination of Landsat-5, Landsat-7, and Landsat-8 from 2002 to 2009 at Xingzi station on Yangtze River (see Materials and Methods). (B and C) Water level measurements are shifted to years 2013–2020 and 1987–1994 in order to explore the effects of NCOs in different time periods. In each panel, the light gray line represents the in situ measured daily water level data. Dots represent valid observations from Landsat on that day (green for observations outside the overlap and pink for extra-observations inside the overlap). Annual changes (line) and their trends (dashed line) of in situ measured data (black color); observations inside the overlap (blue color) and outside the overlap (red color) are also shown, along with the corresponding statistical metrics (R^2, slope of trend, and MAPE). (D) Box plot chart for the relationship between NCOs and the uncertainty of annual mean water level.

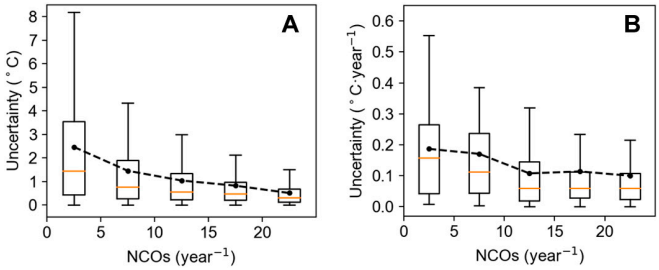

Fig. 12. (A) Box plot chart for the relationship between NCOs and the uncertainty of annual mean WST. (B) Box plot chart for the 10-year trend uncertainty of annual mean WST and NCOs, with the orange line representing the median value and the black dot representing the mean value of each box.

when the number of combined years exceeds 8, the ICO difference tends to stabilize ($\Delta < 0.5\%$). Therefore, it is reasonable for Wang et al. [22] to divide Landsat-5, Landsat-7, and Landsat-8 observations into four periods, 1985–1998, 1999–2006, 2007–2014, and 2015–2020, when studying global changes in ICO.

Discussion

Implications for water environmental studies

Our study discusses the impact of Landsat images on water environmental studies and the potential inaccuracies that can arise due to NCOs. The study finds that even if observations are entirely accurate, annual mean values and multi-year trends of parameters may still be subject to uncertainties. The magnitude of these uncertainties depends on the dynamics of the water environmental parameter and the time period being studied. For example, parameters with small short-term variations, such as water level, exhibit an error of less than 5% when NCOs exceed 10 year^{-1}. On the other hand, parameters that have significant variations in a few days, such as TSS, have a high percentage error of up to ~30%, even with high NCOs.

Our study helps to identify effective strategies for mitigating the impact of NCOs on estimation accuracy. For WST, the error caused by insufficient NCOs remains consistently large and decreases substantially when NCOs >10 year^{-1}. This makes the estimation of WST prone to relatively large errors in most areas during the period when only Landsat-5 is available, except for Australia, Europe, North America, and the overlaps of Asia. After the operation of Landsat-7, the situation has improved, with average NCOs in all other regions exceeding 10 year^{-1}. Since 2014, the simultaneous operation of Landsat-7 and Landsat-8 has greatly increased NCOs, making the annual mean error of almost every statistical location less than 0.5%, and the 10-year trend error less than 0.25 °C year^{-1}. For water level, our study selects in situ data located in Poyang Lake, where the water level has very strong dynamics. The annual mean error is less than 1% only when NCOs are greater than 30 year^{-1}. However, the dynamics of water level in other inland water bodies are likely to be smaller than that of Poyang Lake, and therefore, the associated errors in water level are likely to be smaller. For TSS, the annual mean error can be reduced to a certain extent by increasing NCOs, but it remains at a high level (>10%), and even if NCOs are greater than 30 year^{-1}, the error of annual mean TSS may exceed 20%. This is mainly due to the rapid short-term change of TSS, which can be further compounded by cloud cover during rainfall, reducing NCOs and leading to larger errors. Inland water glacial phenology presents a particularly challenging case for accurate ice phenology estimation using Landsat data. Even by calculating the frequency of ICO, the error may reach 80%. However, combining and calculating multi-year ICO can improve the accuracy of estimations, with the median ICO error becoming stable when the number of combined years is more than eight.

It is worth noting that the four parameters studied in this paper are important indicators of hydrological and water quality changes in inland water bodies. Many other parameters have similar spatiotemporal dynamic characteristics to these four parameters. For example, there is a high correlation between water transparency (turbidity) and TSS [24,25,57–59], lake capacity and water level [27,28,60], water temperature and evaporation [33,61], etc. Therefore, the data presented in our paper are also applicable to the study of these related parameters.

One of the most important finding of this study is that overlap regions between two adjacent swaths greatly increase the NCOs of Landsat, thereby improving the accuracy of

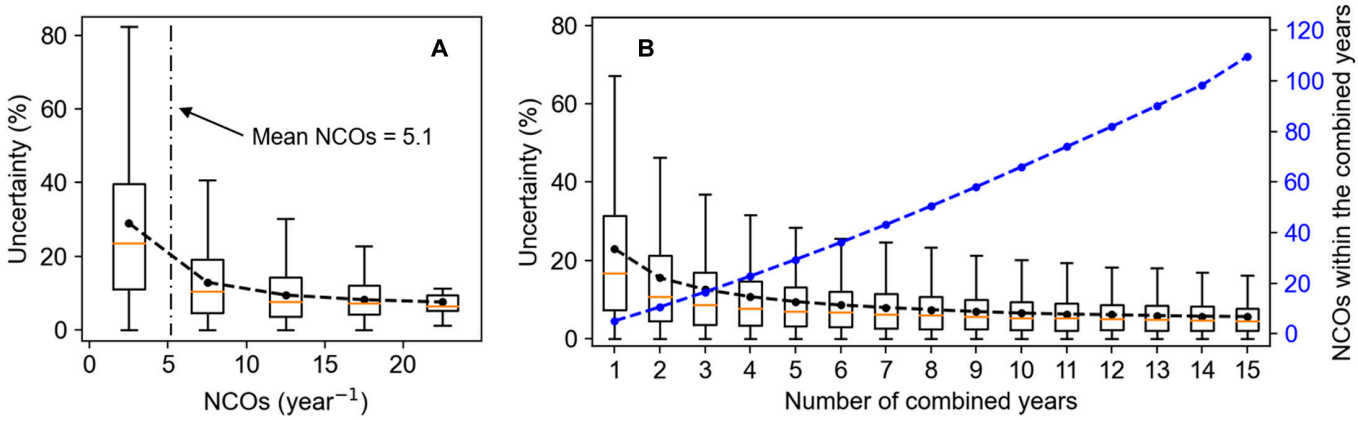

Fig. 13. (A) Box plot chart to show the impacts of NCOs on the uncertainty of ICO at annual scale. The annual mean NCOs of 480 sets of measurement data in this study are depicted by the vertical dotted line. (B) Box plot chart for the uncertainty of ICO and the number of combined years. The NCOs within the combined years are also plotted. In box plot charts, the orange line represents the median value and the black dot represents the mean value of each box.

satellite-based long-term and short-term change detection processes. For parameters with large dynamic changes, such as TSS or lake ice phenologies, we can specifically select data from these overlap regions for long-term change studies. In particular, due to the amplifying effect of global warming [62–64], the water environment in high-latitude regions is facing significant changes, and the large proportion of overlap regions in high-latitude areas can help us better study these changes.

Limitations and recommendations

It should be noted that in our analysis, we assume that the parameters obtained or retrieved from cloud-free Landsat are error-free. However, it is essential to acknowledge that other unfavorable observational conditions, such as sunglint and straylight, can also impact the accuracy of satellite observations for water applications [14,65,66]. Additionally, errors from quantitative inversion model algorithms, atmospheric correction, and other sources can introduce uncertainties into the biogeochemical parameters derived from Landsat data [7,47,67–69]. For example, the uncertainty of TSS inversion algorithms at regional or global scales currently exceeds 30% [70,71], and there are also some uncertainties in obtaining WST, inundation area, ice detection, and other parameters [22,72–74]. Hence, when analyzing water environment change processes using Landsat satellite data, it is essential to consider these sources of errors.

Our study specifically focuses on evaluating the impact of cloud coverage on Landsat observations in water environments. Therefore, our results of the NCOs represent the maximum possible number of valid observations. The uncertainty estimates we provide for corresponding estimations also represent the highest precision achievable by Landsat. We believe that our results are highly valuable for the application of Landsat in water environments. When choosing Landsat as a candidate instrument for specific applications or research, it is recommended that the uncertainty calculated here is smaller than the maximum allowable uncertainty for the given task. Otherwise, achieving the desired accuracy results may be challenging.

Conclusions

We analyzed >4.8 million images acquired from Landsat-5, Landsat-7, and Landsat-8 to understand the global spatiotemporal variations of the NCOs from Landsat missions. We found that Landsat-8 provided almost twice as many mean annual NCOs (21.8 ± 14.7 year^{-1}) compared to Landsat-7 (10.8 ± 4.8 year^{-1}) and Landsat-5 (8.3 ± 5.6 year^{-1}). We also explored the impact of inside/outside overlaps on NCOs and observed that all Landsat observation areas above 45°N had overlapping paths in the east–west direction, enhancing the availability of NCOs. We evaluated the annual mean error and multi-year trend error caused by insufficient NCOs using in situ measured data of four critical water environmental parameters, and the results showed that the uncertainty in retrieving water quality parameters (i.e., TSS) from Landsat is generally higher than that in hydrological parameters (i.e., water level and WST). By evaluating NCOs' impact on water parameter estimations, our study advances the understanding of the limitations and opportunities in utilizing Landsat data for water environmental and hydrological studies.

Acknowledgments

We thank the U.S. Geological Survey for providing Landsat data and Google Earth Engine for providing image-processing resources. We thank the researchers for sharing their valuable open-source databases, including The Global Lake and River Ice Phenology Database, the HydroBASINS database, and the GLAKES database. We thank two anonymous reviewers for their comments and suggestions to improve the quality of this paper.
Funding: This work was supported by the National Natural Science Foundation of China (nos. 42271322 and 42321004) and Guangdong Provincial Higher Education Key Technology Innovation Project (2020ZDZX3006).
Author contributions: L.F. and X.W. designed the experiment and wrote the manuscript.
Competing interests: The authors declare that they have no competing interests.

Data Availability

The Landsat data utilized in this study were provided by the U.S. Geological Survey through Google Earth Engine (https://developers.google.com/earth-engine/datasets/catalog/landsat). The Global Lake and River Ice Phenology Database, employed for validating satellite observations, can be accessed at the National Snow and Ice Data Center (https://nsidc.org/data/G01377/versions/1). The HydroBASINS database was obtained

from https://www.hydrosheds.org/products/hydrobasins, and the GLAKES database was downloaded from https://garslab.com/?p=234.

References

1. Blondeau-Patissier D, Gower JFR, Dekker AG, Phinn SR, Brando VE. A review of ocean color remote sensing methods and statistical techniques for the detection, mapping and analysis of phytoplankton blooms in coastal and open oceans. *Prog Oceanogr*. 2014;123:123–144.
2. Guan Q, Feng L, Hou XJ, Schurgers G, Zheng Y, Tang J. Eutrophication changes in fifty large lakes on the Yangtze plain of China derived from MERIS and OLCI observations. *Remote Sens Environ*. 2020;246:17.
3. Hu CM, Chen ZQ, Clayton TD, Swarzenski P, Brock JC, Muller-Karger FE. Assessment of estuarine water-quality indicators using MODIS medium-resolution bands: Initial results from Tampa Bay, FL. *Remote Sens Environ*. 2004;93(3):423–441.
4. Hu CM, Lee Z, Franz B. Chlorophyll a algorithms for oligotrophic oceans: A novel approach based on three-band reflectance difference. *J Geophys Res Oceans*. 2012;117(C1):C01011.
5. Gardner JR, Yang X, Topp SN, Ross MRV, Altenau EH, Pavelsky TM. The color of rivers. *Geophys Res Lett*. 2021;48(1):e2020GL088946.
6. Kuhn C, Valerio AD, Ward N, Loken L, Sawakuchi HO, Karnpel M, Richey J, Stadler P, Crawford J, Striegl R, et al. Performance of Landsat-8 and Sentinel-2 surface reflectance products for river remote sensing retrievals of chlorophyll-a and turbidity. *Remote Sens Environ*. 2019;224:104–118.
7. Olmanson LG, Brezonik PL, Finlay JC, Bauer ME. Comparison of Landsat 8 and Landsat 7 for regional measurements of CDOM and water clarity in lakes. *Remote Sens Environ*. 2016;185:119–128.
8. Pahlevan N, Chittimalli SK, Balasubramanian SV, Vellucci V. Sentinel-2/Landsat-8 product consistency and implications for monitoring aquatic systems. *Remote Sens Environ*. 2019;220:19–29.
9. Schaeffer BA, Iiames J, Dwyer J, Urquhart E, Salls W, Rover J, Seegers B. An initial validation of Landsat 5 and 7 derived surface water temperature for US lakes, reservoirs, and estuaries. *Int J Remote Sens*. 2018;39(22):7789–7805.
10. Lewis SL, Edwards DP, Galbraith D. Increasing human dominance of tropical forests. *Science*. 2015;349(6250):827–832.
11. Zhao F, Sun R, Zhong L, Meng R, Huang C, Zeng X, Wang M, Li Y, Wang Z. Monthly mapping of forest harvesting using dense time series Sentinel-1 SAR imagery and deep learning. *Remote Sens Environ*. 2022;269:112822.
12. He XQ, Bai Y, Pan DL, Huang NL, Dong X, Chen JS, Chen CTA, Cui QF. Using geostationary satellite ocean color data to map the diurnal dynamics of suspended particulate matter in coastal waters. *Remote Sens Environ*. 2013;133:225–239.
13. Alam SMR, Hossain MS. Probabilities of acquiring cloud-free and low-tide Landsat observations for mapping saltmarsh over South-Eastern Bangladesh from 1980 to 2019. *Mar Geod*. 2023;46(6):562–593.
14. Feng L, Hu C. Comparison of valid ocean observations between MODIS Terra and Aqua over the global oceans. *IEEE Trans Geosci Remote Sens*. 2016;54(3):1575–1585.
15. Zhao D, Feng L. Assessment of the number of valid observations and diurnal changes in Chl-a for GOCI: Highlights for Geostationary Ocean color missions. *Sensors*. 2020;20(12):3377.
16. Feng L, Dai Y, Hou X, Xu Y, Liu J, Zheng C. Concerns about phytoplankton bloom trends in global lakes. *Nature*. 2021;590:E35–E47.
17. Ho JC, Michalak AM, Pahlevan N. Widespread global increase in intense lake phytoplankton blooms since the 1980s. *Nature*. 2019;574(7780):667–670.
18. Hansen MC, Potapov PV, Goetz SJ, Turubanova S, Tyukavina A, Krylov A, Kommareddy A, Egorov A. Mapping tree height distributions in sub-Saharan Africa using Landsat 7 and 8 data. *Remote Sens Environ*. 2016;185:221–232.
19. Kovalskyy V, Roy DP. The global availability of Landsat 5 TM and Landsat 7 ETM+ land surface observations and implications for global 30m Landsat data product generation. *Remote Sens Environ*. 2013;130:280–293.
20. Dai YH, Feng L, Hou XJ, Tang J. An automatic classification algorithm for submerged aquatic vegetation in shallow lakes using Landsat imagery. *Remote Sens Environ*. 2021;260:112459.
21. Pi XH, Luo QQ, Feng L, Xu Y, Tang J, Liang XY, Ma EZ, Cheng R, Fensholt R, Brandt M, et al. Mapping global lake dynamics reveals the emerging roles of small lakes. *Nat Commun*. 2022;13(1):6337.
22. Wang X, Feng L, Gibson L, Qi W, Liu J, Zheng Y, Tang J, Zeng Z, Zheng C. High-resolution mapping of ice cover changes in over 33,000 lakes across the North temperate zone. *Geophys Res Lett*. 2021;48(18):e2021GL095614.
23. Dethier EN, Renshaw CE, Magilligan FJ. Rapid changes to global river suspended sediment flux by humans. *Science*. 2022;376(6600):1447–1452.
24. Feng L, Hu C, Chen X, Song Q. Influence of the three gorges dam on total suspended matters in the Yangtze estuary and its adjacent coastal waters: Observations from MODIS. *Remote Sens Environ*. 2014;140:779–788.
25. Guan Q, Feng L, Tang J, Park E, Ali TA, Zheng Y. Trends in river Total suspended sediments driven by dams and soil erosion: A comparison between the Yangtze and Mekong Rivers. *Water Resour Res*. 2022;58(10):e2022WR031979.
26. Mao Z, Chen J, Pan D, Tao B, Zhu Q. A regional remote sensing algorithm for total suspended matter in the East China Sea. *Remote Sens Environ*. 2012;124:819–831.
27. Cai X, Feng L, Hou X, Chen X. Remote sensing of the water storage dynamics of large lakes and reservoirs in the Yangtze River basin from 2000 to 2014. *Sci Rep*. 2016;6:36405.
28. Feng L, Hu C, Chen X, Li R, Tian L, Murch B. MODIS observations of the bottom topography and its inter-annual variability of Poyang Lake. *Remote Sens Environ*. 2011;115(10):2729–2741.
29. Feng L, Hu C, Chen X, Cai X, Tian L, Gan W. Assessment of inundation changes of Poyang Lake using MODIS observations between 2000 and 2010. *Remote Sens Environ*. 2012;121:80–92.
30. Guo H, Hu Q, Zhang Q, Feng S. Effects of the three gorges dam on Yangtze river flow and river interaction with Poyang Lake, China: 2003–2008. *J Hydrol*. 2012;416–417:19–27.
31. Anderson EJ, Stow CA, Gronewold AD, Mason LA, McCormick MJ, Qian SS, Ruberg SA, Beadle K, Constant SA, Hawley N. Seasonal overturn and stratification changes

drive deep-water warming in one of Earth's largest lakes. *Nat Commun*. 2021;12:1688.
32. Jane SF, Hansen GJA, Kraemer BM, Leavitt PR, Mincer JL, North RL, Pilla RM, Stetler JT, Williamson CE, Woolway RI, et al. Widespread deoxygenation of temperate lakes. *Nature*. 2021;594(7861):66–70.
33. Wang W, Lee XH, Xiao W, Liu SD, Schultz N, Wang YW, Zhang M, Zhao L. Global lake evaporation accelerated by changes in surface energy allocation in a warmer climate. *Nat Geosci*. 2018;11(6):410–414.
34. Woolway RI, Merchant CJ. Worldwide alteration of lake mixing regimes in response to climate change. *Nat Geosci*. 2019;12:271–276.
35. Hou X, Feng L, Dai Y, Hu C, Gibson L, Tang J, Lee Z, Wang Y, Cai X, Liu J, et al. Global mapping reveals increase in lacustrine algal blooms over the past decade. *Nat Geosci*. 2022;15:130–134.
36. Kosten S, Huszar VLM, Becares E, Costa LS, van Donk E, Hansson LA, Jeppesenk E, Kruk C, Lacerot G, Mazzeo N, et al. Warmer climates boost cyanobacterial dominance in shallow lakes. *Glob Chang Biol*. 2012;18(1):118–126.
37. Rigosi A, Hanson P, Hamilton DP, Hipsey M, Rusak JA, Bois J, Sparber K, Chorus I, Watkinson AJ, Qin BQ, et al. Determining the probability of cyanobacterial blooms: The application of Bayesian networks in multiple lake systems. *Ecol Appl*. 2015;25(1):186–199.
38. Christner BC, Priscu JC, Achberger AM, Barbante C, Carter SP, Christianson K, Michaud AB, Mikucki JA, Mitchell AC, Skidmore ML, et al. A microbial ecosystem beneath the West Antarctic ice sheet. *Nature*. 2014;512:310–313.
39. Gronchi E, Jöhnk KD, Straile D, Diehl S, Peeters F. Local and continental-scale controls of the onset of spring phytoplankton blooms: Conclusions from a proxy-based model. *Glob Chang Biol*. 2021;27(9):1976–1990.
40. Hampton SE, Galloway AWE, Powers SM, Ozersky T, Woo KH, Batt RD, Labou SG, O'Reilly CM, Sharma S, Lottig NR, et al. Ecology under lake ice. *Ecol Lett*. 2017;20(1):98–111.
41. Brammer JR, Samson J, Humphries MM. Declining availability of outdoor skating in Canada. *Nat Clim Chang*. 2015;5:2–4.
42. Knoll LB, Sharma S, Denfeld BA, Flaim G, Hori Y, Magnuson JJ, Straile D, Weyhenmeyer GA. Consequences of lake and river ice loss on cultural ecosystem services. *Limnol Oceanogr Lett*. 2019;4(5):119–131.
43. Prowse T, Alfredsen K, Beltaos S, Bonsal BR, Bowden WB, Duguay CR, Korhola A, McNamara J, Vincent WF, Vuglinsky V, et al. Effects of changes in Arctic Lake and river ice. *Ambio*. 2011;40:63–74.
44. Benson, B., J. Magnuson, S. Sharma. Global Lake and River Ice Phenology Database, Version 1 [Data Set]. Boulder (CO): National Snow and Ice Data Center; 2000.
45. Lehner B, Grill G. Global river hydrography and network routing: Baseline data and new approaches to study the world's large river systems. *Hydrol Process*. 2013;27(15):2171–2186.
46. Farr TG, Rosen PA, Caro E, Crippen R, Duren R, Hensley S, Kobrick M, Paller M, Rodriguez E, Roth L, Seal D, Shaffer S, Shimada J, Umland J, Werner M, Oskin M, Burbank D, (2007). The Shuttle Radar Topography Mission. Reviews of Geophysics, 45(2). *Portico*. https://doi.org/10.1029/2005rg000183
47. Zhu Z, Woodcock CE. Object-based cloud and cloud shadow detection in Landsat imagery. *Remote Sens Environ*. 2012;118:83–94.
48. Pekel JF, Cottam A, Gorelick N, Belward AS. High-resolution mapping of global surface water and its long-term changes. *Nature*. 2016;540(7633):418–422.
49. King MD, Platnick S, Menzel WP, Ackerman SA, Hubanks PA. Spatial and temporal distribution of clouds observed by MODIS onboard the Terra and Aqua satellites. *IEEE Trans Geosci Remote Sens*. 2013;51(7):3826–3852.
50. Wertz, J.R. Wertz, J.R. Mission Geometry; Orbit and Constellation Design and Management: *Spacecraft Orbit and Attitude Systems. Springer Netherlands*. 2002;13:985.
51. Loveland TR, Dwyer JL. Landsat: Building a strong future. *Remote Sens Environ*. 2012;122:22–29.
52. Markham BL, Storey JC, Williams DL, Irons JR. Landsat sensor performance: History and current status. *IEEE Trans Geosci Remote Sens*. 2004;42:2691–2694.
53. Wulder MA, Roy DP, Radeloff VC, Loveland TR, Anderson MC, Johnson DM, Healey S, Zhu Z, Scambos TA, Pahlevan N, et al. Fifty years of Landsat science and impacts. *Remote Sens Environ*. 2022;280:113195.
54. Arvidson T, Goward S, Gasch J, Williams D. Landsat-7 long-term acquisition plan: Development and validation. *Photogramm Eng Remote Sens*. 2006;72(10):1137–1146.
55. Ju J, Roy DP. The availability of cloud-free Landsat ETM+ data over the conterminous United States and globally. *Remote Sens Environ*. 2008;112(3):1196–1211.
56. Wang X, Feng L, Qi W, Cai X, Zheng Y, Gibson L, Tang J, Song XP, Liu J, Zheng C, et al. Continuous loss of global Lake ice across two centuries revealed by satellite observations and numerical modeling. *Geophys Res Lett*. 2022;49(12):e2022GL099022.
57. Feng L, Hou X, Zheng Y. Monitoring and understanding the water transparency changes of fifty large lakes on the Yangtze plain based on long-term MODIS observations. *Remote Sens Environ*. 2019;221:675–686.
58. Lagomarsino L, Diovisalvi N, Bustingorry J, Escaray R, Zagarese HE. Diel patterns of total suspended solids, turbidity, and water transparency in a highly turbid, shallow lake (Laguna Chascomús, Argentina). *Hydrobiologia*. 2015;752:21–31.
59. Zhang Y, Qin B, Chen W, Hu W, Yang D. Distribution, seasonal variation and correlation analysis of the transparency in Taihu Lake. *Trans Oceanol Limnol*. 2003;36–39.
60. Cooley SW, Ryan JC, Smith LC. Human alteration of global surface water storage variability. *Nature*. 2021;591:78–81.
61. Lazhu, Yang K, Wang J, Lei Y, Chen Y, Zhu L, Ding B, Qin J. Quantifying evaporation and its decadal change for Lake Nam co, central Tibetan plateau. *J Geophys Res Atmos*. 2016;121(13):7578–7591.
62. Chen XY, Tung KK. Varying planetary heat sink led to global-warming slowdown and acceleration. *Science*. 2014;345(6199):897–903.
63. Cook J, Nuccitelli D, Green SA, Richardson M, Winkler B, Painting R, Way R, Jacobs P, Skuce A. Quantifying the consensus on anthropogenic global warming in the scientific literature. *Environ Res Lett*. 2013;8(2):024024.
64. Ji F, Wu ZH, Huang JP, Chassignet EP. Evolution of land surface air temperature trend. *Nat Clim Chang*. 2014;4:462–466.
65. Goodman JA, Lee Z, Ustin SL. Influence of atmospheric and sea-surface corrections on retrieval of bottom depth and reflectance using a semi-analytical model: A case study in Kaneohe Bay Hawaii. *Appl Opt*. 2008;47(28):F1–F11.

66. Men JL, Tian LQ, Zhao D, Wei JW, Feng L. Development of a deep learning-based atmospheric correction algorithm for oligotrophic oceans. *IEEE Trans Geosci Remote Sens*. 2022;60:4210819.
67. Foga S, Scaramuzza PL, Guo S, Zhu Z, Dilley RD, Beckmann T, Schmidt GL, Dwyer JL, Hughes MJ, Laue B. Cloud detection algorithm comparison and validation for operational Landsat data products. *Remote Sens Environ*. 2017;194:379–390.
68. Liang SL, Fang HL, Chen MZ. Atmospheric correction of landsat ETM+ land surface imagery - part I: Methods. *IEEE Trans Geosci Remote Sens*. 2001;39(11):2490–2498.
69. Young NE, Anderson RS, Chignell SM, Vorster AG, Lawrence R, Evangelista PH. A survival guide to Landsat preprocessing. *Ecology*. 2017;98(4):920–932.
70. Guo J, Ma C, Ai B, Xu X, Huang W, Zhao J. Assessing the effects of the Hong Kong-Zhuhai-Macau bridge on the Total suspended solids in the Pearl River estuary based on Landsat time series. *J Geophys Res Oceans*. 2020;125(8):e2020JC016202.
71. Pahlevan N, Smith B, Alikas K, Anstee J, Barbosa C, Binding C, Bresciani M, Cremella B, Giardino C, Gurlin D, et al. Simultaneous retrieval of selected optical water quality indicators from Landsat-8, Sentinel-2, and Sentinel-3. Remote sensing of environment. *Remote Sens Environ*. 2022;270:112860.
72. Ruiz-Verdu A, Jimenez JC, Lazzaro X, Tenjo C, Delegido J, Pereira M, Sobrino JA, Moreno J, Comparison of MODIS and Landsat-8 retrievals of chlorophyll-a and water temperature over Lake Titicaca. In: *36th IEEE International Geoscience and Remote Sensing Symposium (IGARSS)*. Beijing (People's Republic China): IEEE; 2016. p. 7643–7646.
73. Wang Y, Feng L, Liu JG, Hou XJ, Chen DL. Changes of inundation area and water turbidity of Tonle Sap Lake: Responses to climate changes or upstream dam construction? *Environ Res Lett*. 2020;15(9):0940a1.
74. Yang X, Pavelsky TM, Allen GH. The past and future of global river ice. *Nature*. 2020;577(7788):69–73.